Electric Dipole Moments in a General Two-Higgs Doublet Model

Sven Teunissen

Advisor: Wei-Shu Hou

Graduate Institute of Physics

National Taiwan University

Taipei, Taiwan

June 2024

Abstract

Something something motivation, baryogenesis, cp violation. Something something general two-Higgs doublet model (g2HDM). Something something precision experiments, electric dipole moment (EDM), leptons, quarks.

Contents

List of Figures

List of Tables

Chapter 1

Introduction

One of the biggest unanswered questions of particle physics is that of baryogenesis. Specifically, if electroweak baryogenesis (EWBG) [**?**] were to occur, one would require very large CP violation (CPV) beyond the Standard Model (BSM), since the SM currently houses all its CPV in the CKM matrix [**?**]. However, such large BSM-CPV should have led to new discoveries at the LHC, which evidently is *not* what has been observed. Moreover, in the low-energy precision frontier, electric diploe moments (EDMs) provide a *litmus test* for CPV effects, and experiments have achieved higher and higher precision without discoveries, setting ever more stringent bounds.

Chapter 2

The General Two-Higgs Doublet Model

Following Gell-Mann's *Totalitaian principle*, as a natural extension to the SM, we can introduce a second Higgs doublet. This second doublet couples to all flavors and families of fermions, and has no symmetry requirement imposed upon it. Hence, it is referred to as the "General Two Higgs Doublet Model", or G2HDM for short.

The G2HDM Lagrangian can be written as [**?**, **?**]

$$\mathcal{L} = -\frac{1}{\sqrt{2}} \sum_{f=u,d,\ell} \bar{f}_i \Big[\Big(-\lambda_i^f \delta_{ij} s_\gamma + \rho_{ij}^f c_\gamma \Big) h + \Big(\lambda_i^f \delta_{ij} c_\gamma + \rho_{ij}^f s_\gamma \Big) H - i\,\mathrm{sgn}(Q_f) \rho_{ij}^f A \Big] R\, f_j$$
$$- \bar{u}_i \left[(V\rho^d)_{ij} R - (\rho^{u\dagger} V)_{ij} L \right] d_j H^+ - \bar{\nu}_i \rho_{ij}^L R\, \ell_j H^+ + \mathrm{h.c.}, \tag{2.1}$$

where the generation indices i, j are summed over, L, $R = (1 \pm \gamma_5)/2$ are projections, V is the CKM matrix for quarks and unity for leptons. λ^f are the SM Yukawa matrices, and ρ^f are the extra-Yukawa matrices. A key takeaway is that each family of fermions (u-type, d-type, lepton) is associated with its own extra-Yukawa ρ matrix. In this scenario, flavor-changing neutral Higgs (FCNH) processes are controlled by *flavor hierarchies* and *alignment*. Flavor hierarchies means that the ρ matrices somehow "know" the current flavor structure of the SM,

represented by the "rule of thumb" [**?**]

$$\rho_{ii} \lesssim \mathcal{O}(\lambda_i), \quad \rho_{1i} \lesssim \mathcal{O}(\lambda_1), \quad \rho_{3j} \lesssim \mathcal{O}(\lambda_3), \tag{2.2}$$

with $j \neq 1$. Alignment means that $c_\gamma \equiv \cos\gamma = \cos(\beta - \alpha)$ is small. Consequently, the SM-like Higgs h is mostly controlled by the SM Yukawas, while the newly introduced ρ matrices control the exotic Higgses $H, A, H^\pm$. A remarkable feature of G2HDM is that $\mathcal{O}(1)$ ρ_{tt} can drive EWBG through [**?**] $\lambda_t \mathrm{Im}\rho_{tt}$.

Chapter 3

Electric Dipole Moment

The effective interaction term that produces EDM d_f for a fermion f is the dimension-5 operator

$$-\frac{i}{2}d_f\left(\bar{f}\sigma^{\mu\nu}\gamma_5 f\right)F_{\mu\nu}. \tag{3.1}$$

In G2HDM, the first finite contribution to EDM appears at one-loop. The dipole operator is chirality violating, so an additional mass insertion is required on the fermion line to obtain the correct chiral structure. This means that those one-loop diagrams with lighter leptons in the loop are chirally suppressed. The next contribution to this operator is the two-loop Barr-Zee diagram. Naively, one would directly assume these to be loop-suppressed. However, the two-loop diagram having only one chirality flip, compared to three chirality flips for the one-loop diagram, effectively compensates for the loop suppression.

It is straightforward yet tedious to calculate the two-loop Barr-Zee diagrams analytically, but it can be done nonetheless, as seen in the original paper by Barr and Zee [**?**] for neutral scalar contributions with a top quark or gauge boson in the loop, as well as later extensions [**?**] to other loop diagrams. The final formulae for the various Barr-Zee diagrams are as follows, following the notations of [**?**],

$$(d_l^{\phi G})_t = -\frac{e\,m_l}{(4\pi)^4}\sqrt{2}G_F \sum_{\phi=h,H,A}\sum_{G=\gamma,Z} N_c Q_t (g^L_{Gll}+g^R_{Gll}) \times\left[\frac{g^A_{\phi ll}}{m_l/v}\frac{g^V_{\phi tt}}{m_t/v}\mathcal{I}_1^G(m_t,m_\phi)+\frac{g^V_{\phi ll}}{m_l/v}\frac{g^A_{\phi tt}}{m_t/v}\mathcal{I}_2^G(m_t,m_\phi)\right] \tag{3.2}$$

where

$$\mathcal{I}_1^G(m_t,m_\phi) = (g^L_{Gtt}+g^A_{Gtt})\frac{m_t^2}{m_\phi^2-m_G^2}\left(-2\frac{m_G^2}{m_t^2}f\left(\frac{m_t^2}{m_G^2}\right)+2\frac{m_\phi^2}{m_t^2}f\left(\frac{m_t^2}{m_\phi^2}\right)\right)$$
$$\mathcal{I}_2^G(m_t,m_\phi) = (g^L_{Gtt}+g^A_{Gtt})\frac{m_t^2}{m_\phi^2-m_G^2}\left(-2\frac{m_G^2}{m_t^2}g\left(\frac{m_t^2}{m_G^2}\right)+2\frac{m_\phi^2}{m_t^2}g\left(\frac{m_t^2}{m_\phi^2}\right)\right) \tag{3.3}$$

$$(d_l^{\phi G})_W = +\frac{e\,m_l}{(4\pi)^4}\sqrt{2}G_F \sum_{\phi=h,H,A}\sum_{G=\gamma,Z} (g^L_{Gll}+g^R_{Gll})\frac{g^A_{\phi ll}}{m_l/v}\frac{g_{WW\phi}}{2m_W^2/v}\mathcal{I}_W^G(m_\phi) \tag{3.4}$$

where

$$\mathcal{I}_W^G(m_\phi) = g_{WWG}\frac{2m_W^2}{m_\phi^2-m_G^2} \times\left[-\frac{1}{4}\left\{\left(6-\frac{m_G^2}{m_W^2}\right)+\left(1-\frac{m_G^2}{2m_W^2}\right)\frac{m_\phi^2}{m_W^2}\right\}\left[-2\frac{m_\phi^2}{m_W^2}f\left(\frac{m_W^2}{m_\phi^2}\right)+2\frac{m_G^2}{m_W^2}f\left(\frac{m_W^2}{m_G^2}\right)\right]\right.$$
$$\left.+\left\{\left(-4+\frac{m_G^2}{m_W^2}\right)+\frac{1}{4}\left(\left(6-\frac{m_G^2}{m_W^2}\right)+\left(1-\frac{m_G^2}{2m_W^2}\right)\frac{m_\phi^2}{m_W^2}\right)\right\}\left[-2\frac{m_\phi^2}{m_W^2}g\left(\frac{m_W^2}{m_\phi^2}\right)+2\frac{m_G^2}{m_W^2}\right. \tag{3.5}$$

$$(d_l^{\phi G})_{H^\pm} = +\frac{e\,m_l}{(4\pi)^4}\sqrt{2}G_F \sum_{\phi=h,H,A}\sum_{G=\gamma,Z} (g^L_{Gll}+g^R_{Gll})\frac{g^A_{\phi ll}}{m_l/v}\frac{g_{\phi H^+H^-}}{v}\mathcal{I}_3^G(m_{H^\pm},m_\phi) \tag{3.6}$$

where

$$\mathcal{I}_3^G(m_{H^\pm},m_\phi) = -\frac{1}{2}g_{GH^+H^-}\frac{v^2}{m_\phi^2-m_G^2} \times\left[\left(-2\frac{m_G^2}{m_{H^\pm}^2}f\left(\frac{m_{H^\pm}^2}{m_G^2}\right)+2\frac{m_\phi^2}{m_{H^\pm}^2}f\left(\frac{m_{H^\pm}^2}{m_\phi^2}\right)\right)-\left(-2\frac{m_G^2}{m_{H^\pm}^2}g\left(\frac{m_{H^\pm}^2}{m_G^2}\right)+2\frac{m_\phi^2}{m_{H^\pm}^2}g\left(\frac{m}{r}\right.\right.\right. \tag{3.7}$$

$$(d_l^{H^+W^+})_{t/b} = \tag{3.8}$$

$$(d_l^{H^+W^+})_W = \tag{3.9}$$

$$(d_l^{H^+W^+})_{H^+} = \tag{3.10}$$

with loop functions

$$\begin{aligned} f(a) &= \frac{1}{2}a\int_0^1 \mathrm{d}z\, \frac{1-2z(1-z)}{z(1-z)-a}\log\frac{z(1-z)}{a} \\ g(a) &= \frac{1}{2}a\int_0^1 \mathrm{d}z\, \frac{1}{z(1-z)-a}\log\frac{z(1-z)}{a} \end{aligned} \tag{3.11}$$

$$\begin{aligned} T(a) &= \\ B(a) &= \end{aligned} \tag{3.12}$$

For quarks, they participate in the strong interaction, so there will be QCD-related effects. This can be found in two additional terms in the Lagrangian: the chromo-EDM $\tilde{d}_f$ for fermion f, and the Weinberg term C_W for gluon interactions [**?**], written as

$$-\frac{ig_s}{2}\tilde{d}_f\left(\bar{f}\sigma^{\mu\nu}T^a\gamma_5 f\right)G^a_{\mu\nu} \qquad\qquad -\frac{1}{3}C_W f^{abc}G^a_{\mu\sigma}G^{b,\sigma}_{\nu}\tilde{G}^{c,\mu\nu} \tag{3.13}$$

The formulae for calculating the cEDM are

$$\tilde{d}_f = \tag{3.14}$$

$$C_W = \tag{3.15}$$

The contribution of the Weinberg diagram can be evaluated using QCD running.

$$\frac{d_f(\mu_h)}{2} = \tag{3.16}$$

$$\frac{\tilde{d}_f(\mu_h)}{2} = \tag{3.17}$$

$$C_W(\mu_h) = \tag{3.18}$$

where constants.

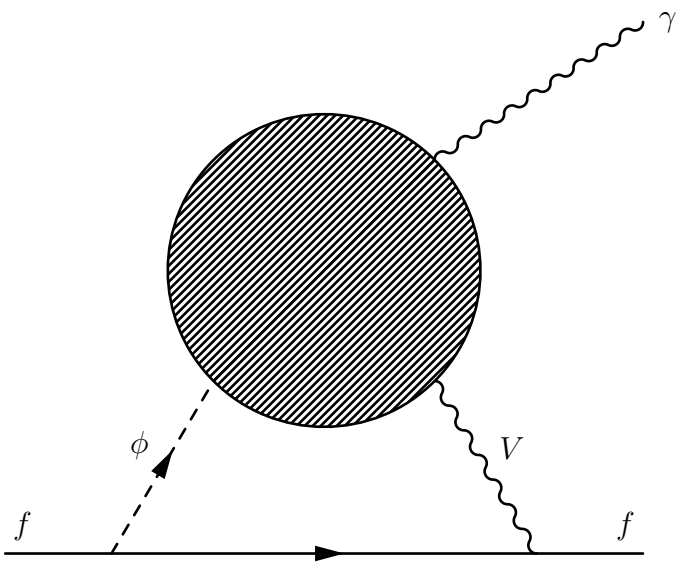

Figure 3.1: Two-loop Barr-Zee diagram

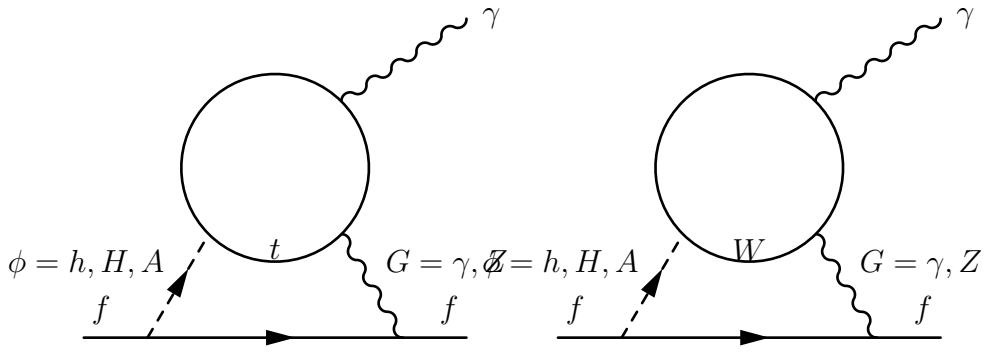

(a) Neutral Higgs, top loop

(b) Neutral Higgs, W loop

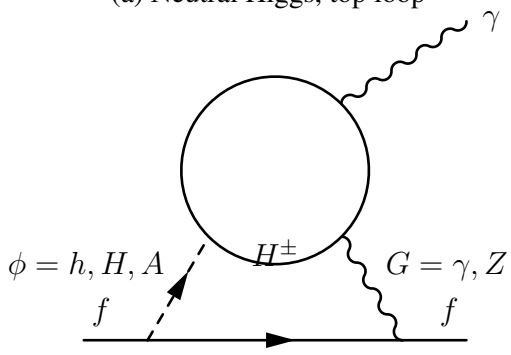

(c) Neutral Higgs, charged Higgs loop

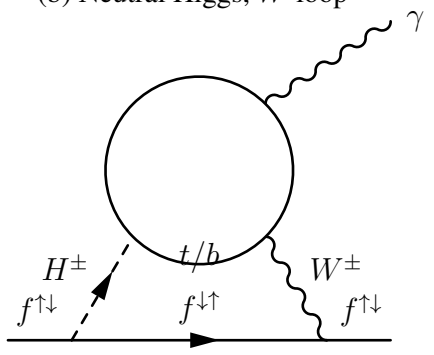

(d) Charged Higgs, top/bottom loop

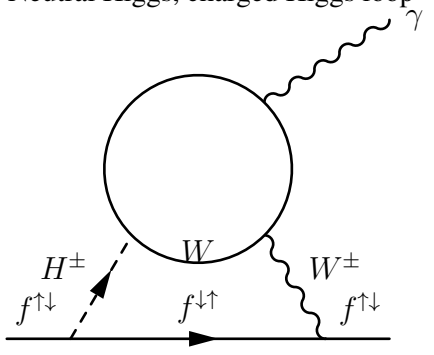

(e) Charged Higgs, W loop

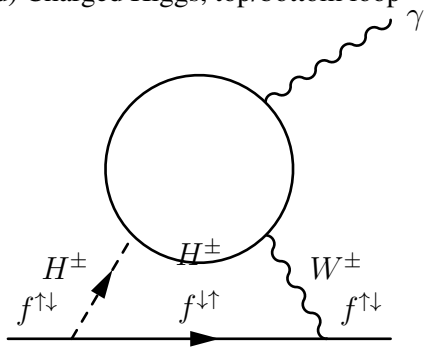

(f) Charged Higgs, charged Higgs loop

Figure 3.2: Specific Two-loop Barr-Zee diagrams

Chapter 4

Electric Dipole Moment of Leptons

Naturally, following the framework laid out previously, we want to perform calculations on the various leptons. A brief review of past experimental results shows that the experimental development of electron EDM (eEDM) over the past few years has been remarkably rapid. Just earlier last year, JILA [**?**] has surpassed the previous bound from ACME [**?**] and pushed the precision of eEDM down to $|d_e| < 4.1 \times 10^{-30}\, e\,\mathrm{cm}$. It is noteworthy to point out that these eEDM experiments are relatively small in scale, "tabletop experiments" even when compared to behemoths like the LHC, which makes the extreme precision achieved all the more impressive. For the electron, an extensive study of eEDM in G2HDM can be found in the 2018 and 2020 papers of Fuyuto, Senaha, and Hou (Refs. [**?**]). Our investigation on eEDM is essentially an extension of the 2020 paper to a larger parameter space.

As mentioned before, one big motivation for G2HDM as a viable model is the fact that $\mathcal{O}(1)\rho_{tt}$ can drive baryogenesis through $\lambda_t \mathrm{Im}\rho_{tt}$. However, this same ρ_{tt}, along with ρ_{ff} for a given fermion f, also generates EDM for said fermion. We thus arive at a "point of tension" between theory and experiment: we desire a large ρ_{tt} for baryogenesis, but need a small ρ_{tt} to survive precision bounds on various EDMs. Electron EDM, in particular, is a great "observable of contention", since experiments measuring it are the most precise compared to other EDMs. In an

attempt to address this issue, Fuyuto, Senaha, and Hou proposed a "cancellation ansatz" between ρ_{ee} and ρ_{tt}

$$\mathrm{Re}\rho_{ee} = -r\frac{\lambda_e}{\lambda_t}\mathrm{Re}\rho_{tt}, \quad \mathrm{Im}\rho_{ee} = +r\frac{\lambda_e}{\lambda_t}\mathrm{Im}\rho_{tt}, \tag{4.1}$$

that allows for small values of eEDM while keeping a *sizeable* ρ_{tt}. The r depends on the loop functions from the previous chapter. This ansatz signifies two key points. First, it gives a flavor hierarchy $|\rho_{ee}|/|\rho_{tt}| \sim \lambda_e/\lambda_t$ that reflects SM. Second, it represents a phase lock between ρ_{ee} and ρ_{tt}. This ansatz results in a "dip" in eEDM around the r value of ~ 0.7, which is when the W-loop and the top-loop in the Barr-Zee diagram effectively cancel each other out. This provides a mechanism for the eEDM in G2HDM to be small and evade the experimental bounds while not directly modifying ρ_{tt}. When revisiting their study, we found the assumptions on the value of ρ_{tt} to be quite "conservative", setting $\mathrm{Re}\rho_{tt} = \mathrm{Im}\rho_{tt} = -0.1$ (which equates to $|\rho_{tt}| = 0.1\sqrt{2} \approx 0.14$). We believe that might be due to *playing it safe* under the pressure of the rapid advancements on the experimental front. In our study [**?**], we *push against the boundary*, and explore a larger range of ρ_{tt}, up to $\mathrm{Re}\rho_{tt} = \mathrm{Im}\rho_{tt} = -0.3$ ($|\rho_{tt}| = 0.3\sqrt{2} \approx 0.42$). We want to see how big we can keep the parameter space for baryogenesis while still satisfying precision constraints. As mentioned before, one of the key points of G2HDM is the *flavor hierarchy*, illustrated by the *rule of thumb* (2.2). This "cancellation ansatz" happens to capture the idea of such a hierarchy pretty well from a numerical standpoint; so, for the sake of numerical illustration of the flavor hierarchy, we extend the ansatz to all fermion ρ_{ff}s, except for the top itself:

$$\mathrm{Re}\rho_{ff} = -r\frac{\lambda_f}{\lambda_t}\mathrm{Re}\rho_{tt}, \quad \mathrm{Im}\rho_{ff} = +r\frac{\lambda_f}{\lambda_t}\mathrm{Im}\rho_{tt}. \tag{4.2}$$

We must reiterate that this is merely a move of convenience, and the actual values of the ρ_{ff}s need not precisely match this ansatz. Results are shown in Figure 4.1.

For the sake of clarity, we have taken a slight liberty in illustrating the range of the purple "allowed window" band, using the left- and right-most curves instead of the left and right side of a given curve. Nevertheless, the trend we wish to describe

is not affected by such. From our results, it can be seen that as $|\rho_{tt}|$ increases, the allowed window of the proportionality parameter r shrinks, yet there is still a decent range of acceptable probable values. $\mathrm{Re}\rho_{tt} = \mathrm{Im}\rho_{tt} = -0.1$ was indeed a conservative representative value, and $\mathrm{Re}\rho_{tt} = \mathrm{Im}\rho_{tt} = -0.3$ may still be a viable option in the baryogenesis parameter space.

After the electron, we move on to its slightly heavier cousin, the muon. Since the bound on the muon is not as strong, one does not need to resort to the cancellation ansatz immediately. Instead, we perform a scan of the ρ_{tt} parameter space for a representative $\rho_{\mu\mu}$ value, and see how it affects the μEDM. Results are shown in Figure 4.2.

We see that there is still a "cancellation dip" for the neutral scalar-attached loops, which arises from the opposite signs of the W-loop and the top-loop. The details of said cancellation is exactly the same as that of the electron. Our predicted values for μEDM are still two to three orders of magnitude below the current bounds, so we are eager to see development on the experimental front. Once the bounds close in, it may also be fruitful to consider the "cancellation ansatz" on the muon as well, especially since the leptons share a extra Yukawa matrix ρ^l, which makes it more likely that the ρ_{ll} might exhibit similar relationships with ρ_{tt}.

Lastly, we analyze the heaviest lepton, the tau. On the experiment front, the precision of tauEDM measurements are still pretty low. We perform the same calculations as the muon, with $\rho_{\mu\mu} = i\lambda_\mu$ replaced by $\rho_{\tau\tau} = i\lambda_\tau$. Results are shown in Figure 4.3

As seen in Figure 4.3, our predicted values are still several orders of magnitude below current experimental results. Further precision or methodology improvements are required for a more fruitful analysis of tauEDM, so we just present our results here without much further comment.

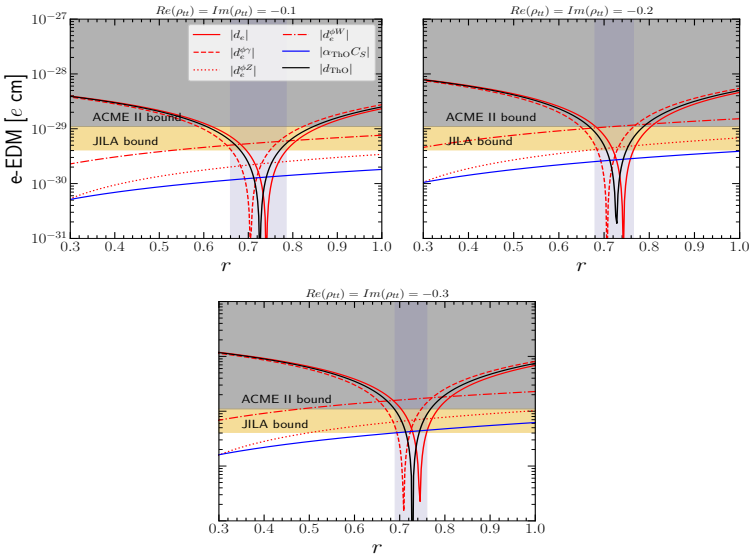

Figure 4.1: eEDM v.s. r for a larger range of ρ_{tt} with ansatz Eq. (4.2). ($c_\gamma = 0.1, m_{H,A,H^+} = 500\,\text{GeV}$)

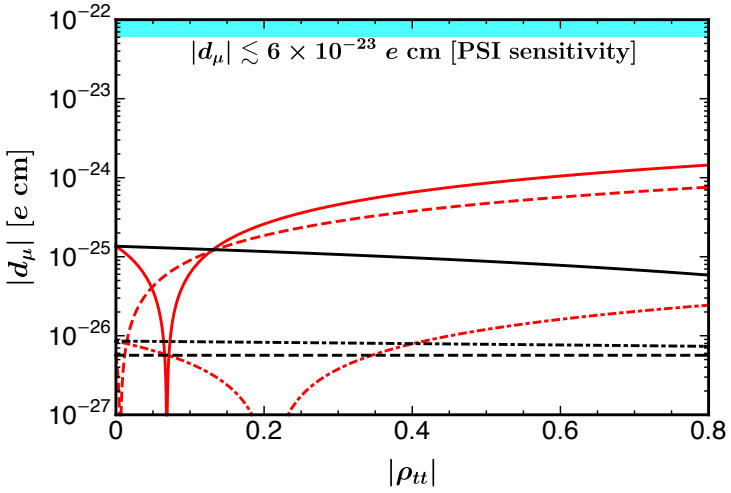

Figure 4.2: μEDM results.

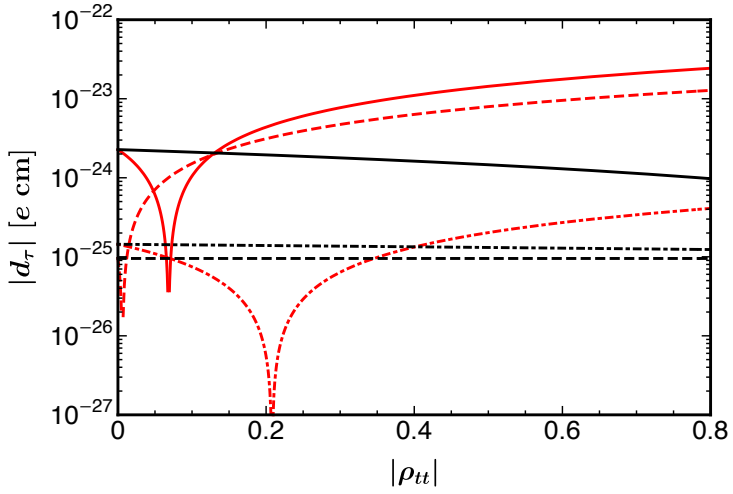

Figure 4.3: τEDM results.

Chapter 5

Electric and Chromo-electric Dipole Moment of Quarks

After the analysis for leptons, we turn our gaze towards EDMs involving quarks. As mentioned in the theory section, there are additional chromo-EDM and Weinberg term contributions to take into account that arise from the fact that quarks interact via QCD. However, since quarks are always confined as hadrons, it is extremely difficult, if not outright impossible, to directly probe the EDMs of individual quarks, given the state of current technology and our understanding of QCD. A quick literature review shows that there are indeed no direct experimental observations for the EDMs of all the quarks lighter than the top quark. As for the top quark, there has been experimental progress at CMS to constrain the value of its chromo-EDM, as seen in Refs. [**?**] and [**?**]. This, in fact, was our original motivation for exploring quark EDMs in G2HDM. Alas, the constraints imposed by the aforementioned analyses are still relatively weak, so we do not pursue this observable any further for the moment. We do want to keep an eye out for further experimental developments on this front, though. It is natural, under these circumstances, to shift our attention towards hadron EDMs, and utilize the EDM of hadrons to observe the effect of the EDMs of individual quarks. The prime candidate in this case would be the neutron EDM (nEDM).

Neutron EDM measurements have been in the experimental realm for quite some time already. The most recent results are given by PSI [**?**] in 2020, setting the bound at $|d_n| < 1.8 \times 10^{-26}\ e\,\mathrm{cm}$. A recent report from the Snowmass conference [**?**] has shed some light on the past, present, and future of nEDM experiments. As can be seen from Figure 5.1 taken from said report [**?**], progress on the nEDM front has stagnated for a decade or so, with the precision plateauing at $\sim 10^{-26}\ e\,\mathrm{cm}$. However, projects to improve the sensitivity are already in the works, so it is still worth to explore the nEDM parameter space.

We use the recent formula [**?**]

$$d_n = -0.20\, d_u + 0.78\, d_d + e\,(0.29\, \tilde{d}_u + 0.59 \tilde{d}_d) + e\, 23\ \mathrm{MeV}\, C_W \tag{5.1}$$

to estimate the nEDM. We evaluate the contributions to $\tilde{d}_{u,d}$ and C_W in G2HDM by following Refs. [**?**] and [**?**], with discussion on theoretical uncertainties found in Ref. [**?**]. We present the results for nEDM in Figure 5.2, as well as combined results for eEDM and nEDM in the range $r \in [0.6, 0.8]$ in Figure 5.3, with the "extended" ansatz (4.1) applied.

Interestingly, our predictions for nEDM are not too far below the current experimental bound. We see that, even for $|\rho_{tt}| = 0.3\sqrt{2} \approx 0.42$, one can still survive the current PSI bound. In the combined plot, the eEDM cancellation mechanism from the previous section at $r \approx 0.7$ clearly illustrated. The interplay of the nEDM and the eEDM in Figure 5.3 shows that our predictions are of notable significance in both precision observables. The follow-up project at PSI, named n2EDM [**?**], plans to reach a sensitivity of $\sim 10^{-27}\ e\,\mathrm{cm}$ within a decade, which covers the range illustrated in Figure 5.2.

We have been utilizing the "extended" cancellation ansatz (4.1) in our above calculations and analyses, but we have to stress that, as described before, it is merely a convenient way to numerically illustrate the *flavor hierarchy* of the G2HDM. A closer examination of the "extended" ansatz reveals a logical flaw: since ρ_{uu} and ρ_{tt} are in the same ρ matrix, and the ansatz obviously does not hold for ρ_{tt} itself, there is no reason to expect it to hold for ρ_{uu}. Thus, for this situation, we should

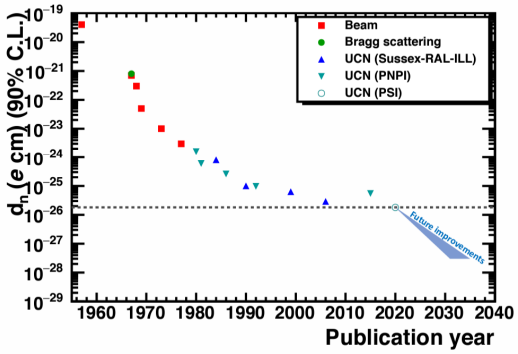

Figure 5.1: nEDM experimental progress [**?**]

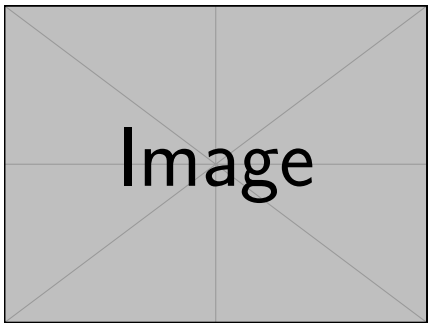

Figure 5.2: nEDM results.

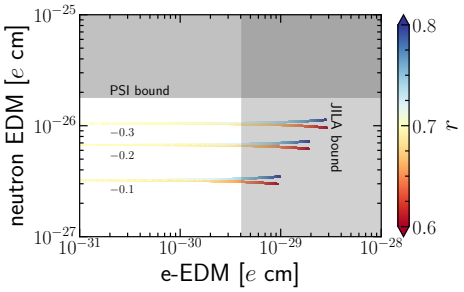

Figure 5.3: Combined eEDM-nEDM result.

fall back one step, and rely on the *rule of thumb* (2.2) instead of the ansatz. Hence, we relax the ansatz for ρ_{uu}, and explore the range of $\mathcal{O}(\lambda_u)$ by varying

$$|\rho_{uu}| \in [0.3\lambda_u, 3\lambda_u], \quad \arg \rho_{uu} \in [-\pi, \pi] \tag{5.2}$$

while keeping the other ρ_{ff}s intact, i.e. still following the ansatz. We present our results in Figure 5.4.

The different colors of the points represent different values of $\arg \rho_{uu}$, and an interesting pattern can be seen among them. The red points have negative $\arg \rho_{uu}$, which is the same sign as ρ_{tt}; the nEDM of these points are larger, but stay mostly below the PSI bound. On the other hand, the blue points have *positive* $\arg \rho_{uu}$, which is the *opposite* sign as ρ_{tt}; remarkably, the value of nEDM of these points drop significantly, reaching as low as $10^{-28}\ e\,\mathrm{cm}$ or lower, evading even the projected sensitivity of n2EDM at PSI! This phenomenon in Figure 5.4 illustrates a *natural* cancellation mechanism present within the dynamics of nEDM, arising from the phase difference of ρ_{uu} and the other ρ_{ff}. Even though this mechanism can evade the projected n2EDM sensitivity, it can still be probed by future experiments, such as the Spallation Neutron Source (SNS) at Oak Ridge National Laboratory (ORNL) [**?**], which can reach sensitivities down to $\sim 10^{-28}$ $e\,\mathrm{cm}$. This experiment may take more than a decade to come to fruition, but it almost fully covers our projected range, since the blue dots are still mostly concentrated above $10^{-28}\ e\,\mathrm{cm}$.

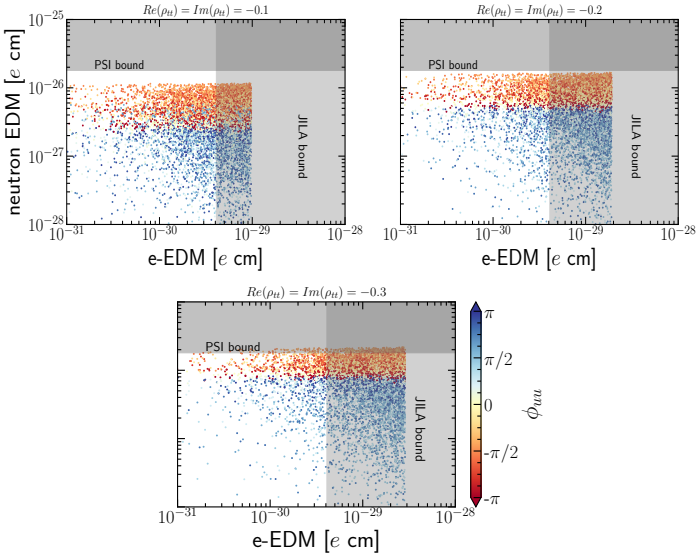

Figure 5.4: Results for eEDM and nEDM with $|\rho_{uu}| \sim \lambda_u$.

Chapter 6

Conclusion

Some comments, perhaps regarding the masses and degeneracy of the heavy Higgses.

We present an analysis of various EDMs of fundamental particles in the framework of a G2HDM. We note that to evade precision bounds while satisfying the conditions for baryogenesis, a cancellation is possible, which is also an indicator of an underlying *flavor hierarchy*. This is most prevalent in eEDM, where bounds are the strongest, and experimental precision improving rapidly. We analyze muEDM, with our predictions still being a couple orders of magnitude below current experimental bounds. We present results for tauEDM, but provide no further analysis since the bounds are still too imprecise. We analyze quark EDM through nEDM, and optain promising prospective results, especially when viewed together with eEDM. We stress that this is a noteworthy area to pay attention to in the upcoming decade or two.

Reference